PHYSICAL REVIEW B **95**, 241101(R) (2017)

Global band topology of simple and double Dirac-point semimetals

Adrien Bouhon* and Annica M. Black-Schaffer
Department of Physics and Astronomy, Uppsala University, Box 516, SE-751 21 Uppsala, Sweden
(Received 17 February 2017; published 5 June 2017)

We combine space group representation theory together with the scanning of closed subdomains of the Brillouin zone with Wilson loops to algebraically determine the global band-structure topology. Considering space group No. 19 as a case study, we show that the energy ordering of the irreducible representations at the high-symmetry points $\{\Gamma,S,T,U\}$ fully determines the global band topology, with all topological classes characterized through their simple and double Dirac points.

DOI: 10.1103/PhysRevB.95.241101

Topological semimetals with their protected band-crossing Dirac (or Weyl) points have recently attracted a lot of interest. As many other topological phases of matter, symmetries play an important role in the understanding, classification, and prediction of topological semimetals [1]. While much work have focused on the local characterization of symmetry-protected Dirac points [2–7] and also on specific global features [8–17], a systematic treatment of the global band topology enforced by the crystal space group is still missing.

Space group representation theory fully determines the symmetry-protected band crossings occurring at high-symmetry points or lines of the Brillouin zone (BZ), each being treated separately [18]. It was also realized early on that nonsymmorphic space groups can realize *connected elementary energy bands* [19–22], i.e., a minimum number of bands that are connected through enough contact points such that one can travel continuously through these bands over the BZ. This leads to an additional global type of symmetry-protected Dirac points that can be moved in some determined regions of the BZ but are globally unavoidable. A consequence for such space groups is the tightening of the necessary electron filling condition for realizing a band insulator. While the filling number must usually only be even for a insulating state, it typically needs to be within a proper subset of this for a nonsymmorphic space group [23]. Conversely, it is sufficient (but not necessary) to violate this tighter filling condition to achieve a semimetallic phase.

Still, one main question has remained open so far: For a given space group $\mathcal{G}$, what is the global topology of the band structure including all Dirac points, which in turn also provides the filling condition for a topological semimetallic state? In this Rapid Communication we show that combining space group representation theory together with Wilson loop techniques to calculate the Berry phase leads to a definitive answer to the question, using space group No. 19 (SG19) as a case study [24]. In fact, we show that the global band topology, including all symmetry-protected Dirac points, is fully determined simply by the energy ordering of the irreducible representations (IRREPs) at the high-symmetry points $\{\Gamma,S,T,U\}$.

4N-band structures in sg19. The nonsymmorphic SG19 ($P2_12_12_1$) is composed of a primitive orthorhombic Bravais lattice and three screw axes $\{g|\boldsymbol{\tau}_g\}$ with the point group elements $g \in D_2 = \{E,C_{2z},C_{2y},C_{2x}\}$ and the fractional translations $\boldsymbol{\tau}_x = (\boldsymbol{a}_1+\boldsymbol{a}_2)/2$, $\boldsymbol{\tau}_y = (\boldsymbol{a}_2+\boldsymbol{a}_3)/2$, $\boldsymbol{\tau}_z = (\boldsymbol{a}_1+\boldsymbol{a}_3)/2$, where $\{\boldsymbol{a}_i\}_{i=1,2,3}$ are the primitive lattice vectors. Since SG19 has a single Wyckoff position with no symmetry, the set of all [one-dimensional (1D)] IRREPs at Γ must split into N copies of the four IRREPs of D_2, $\{\Gamma_1^{\mathbf{0}},\Gamma_2^{\mathbf{0}},\Gamma_3^{\mathbf{0}},\Gamma_4^{\mathbf{0}}\}$ defined by the character table in Fig. 1(b) [25]. Likewise, the set of all two-dimensional (2D) IRREPs at the points $U_i \in \{S,T,U\}$ splits into N copies of the two projective IRREPs $\{\Gamma_5^{U_i},\Gamma_6^{U_i}\}$, also given in Fig. 1(b) [18,26]. It is convenient to split the high-symmetry lines into three distinct BZ subspaces: $\mathcal{B}_\Gamma = \bigcup_{X_i=X,Y,Z} \overline{\Gamma X_i}$ (high-symmetry lines crossing Γ), $\mathcal{B}_R = \bigcup_{U_i} \overline{RU_i}$ (high-symmetry lines crossing R), and $\mathcal{B}_{\Gamma\text{-}R} = \bigcup_{X_i,U_i} \overline{X_iU_i}$ (high-symmetry lines connecting $\mathcal{B}_\Gamma$ and $\mathcal{B}_R$) [see Fig. 1(a)]. Only a unique 2D IRREP is allowed on $\mathcal{B}_{\Gamma\text{-}R}$ [18,26]. This leads to $\mathcal{B}_\Gamma$ and

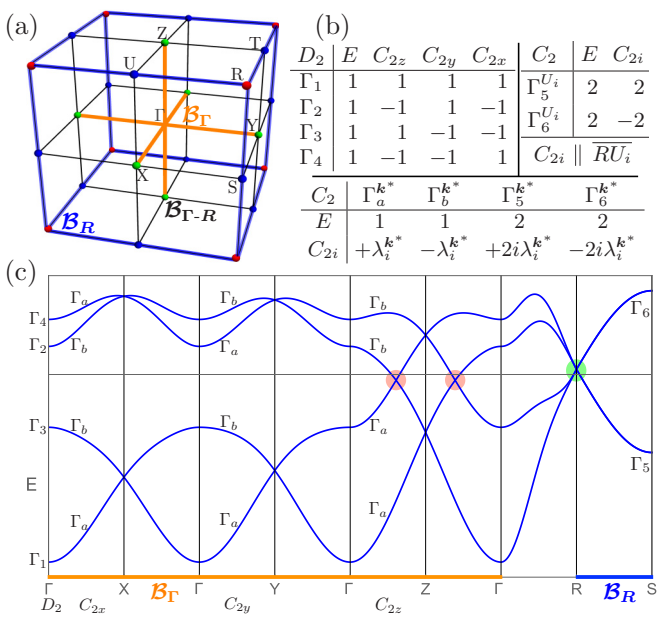

FIG. 1. (a) BZ with high-symmetry points and lines of SG19. (b) Character tables of the IRREPs for the point groups D_2 and C_2 with $\lambda_i^{\boldsymbol{k}^*} = e^{-i\boldsymbol{k}^*\cdot\boldsymbol{\tau}_i}$, where $\boldsymbol{k}^*$ belongs to one line of $\mathcal{B}_\Gamma$ for $\{\Gamma_a,\Gamma_b\}$ and $\mathcal{B}_R$ for $\{\Gamma_5,\Gamma_6\}$. (c) Electronic band structure of a four-band tight-binding model in SG19. Unavoidable globally protected simple Dirac points ($|C_1| = 1$) in red and double Dirac point ($|C_1| = 2$) in green.

*adrien.bouhon@physics.uu.se

TABLE I. Band permutation rules in $\mathcal{B}_\Gamma$ and $\mathcal{B}_R$. Bands are labeled according to their IRREPs at Γ for $\mathcal{B}_\Gamma$ and U_i for $\mathcal{B}_R$.

$\mathcal{P}_{\overline{\Gamma b_1}}$	$\mathcal{P}_{\overline{\Gamma b_2}}$	$\mathcal{P}_{\overline{\Gamma b_3}}$	$\mathcal{P}_{\overline{Sb_3}},\mathcal{P}_{\overline{Tb_1}},\mathcal{P}_{\overline{Ub_2}}$
(12)(34)	(13)(24)	(12)(34)	(56)
(13)(24)	(14)(23)	(14)(23)	

$\mathcal{B}_R$ being *symmetry independent* since their IRREPs are not constrained by their compatibility relation into $\mathcal{B}_{\Gamma\text{-}R}$.

With this background we directly state our first main result: *Any $4N$-band structure of SG19 can be reconstructed by hand from the list of energy-ordered IRREPs at the high-symmetry points $\{\Gamma,S,T,U\}$ by applying rules 1–4 below.* To show this, we start with the $\mathcal{B}_\Gamma$ subspace. Labeling all the energy eigenvalues at Γ according to their band index ($n=1,\ldots,N$) and IRREP ($j=1,2,3,4$) as $E^n_j(\mathbf{0})$, we can follow smoothly each eigenvalue branch over $\mathcal{B}_\Gamma$ [we define this as the *smooth gauge*; see Supplemental Material (SM) [27]]. We write $\mathcal{P}_{\overline{\Gamma b_i}}=(j_1j_2)(j_3j_4)$ for the two-by-two permutation in energy of the four bands $\{E^{n_1}_{j_1},E^{n_2}_{j_2},E^{n_3}_{j_3},E^{n_4}_{j_4}\}$ under a shift by a primitive reciprocal lattice vector $\boldsymbol{b}_i$ ($\boldsymbol{b}_i \parallel \overline{\Gamma X_i}$). We then get (see SM [27]) *rule 1: All bands are permuted along each line of $\mathcal{B}_\Gamma$ according to Table I.*

Permutations only happen between bands belonging to different IRREPs along each line $\overline{\Gamma X_i}$, i.e., with different compatibility relations $\Gamma^{\mathbf{0}}_j \to \Gamma^{\boldsymbol{k}^*\in\overline{\Gamma X_i}}_k, k=a,b$ [see Fig. 1(b)]. Hence, any two permuted bands have a symmetry-protected crossing. In fact, these crossing points are at the middle points $\{X,Y,Z\}$ because of their D_2 symmetry [18,26,28]. In addition, we have *rule 2: For any two bands $E^{n_1}_{j_1}$ and $E^{n_2}_{j_2}$ at Γ with the same compatibility relation into $\overline{\Gamma X_i}$, we have*

$$E^{n_1}_{j_1}(\mathbf{0}) \gtrless E^{n_2}_{j_2}(\mathbf{0}) \Leftrightarrow E^{n_1}_{j_1}(\boldsymbol{k}^*) \gtrless E^{n_2}_{j_2}(\boldsymbol{k}^*), \quad \forall \boldsymbol{k}^* \in \overline{\Gamma X_i}.$$

This rule is a straightforward consequence of (i) the smoothness of the eigenvalues as functions of $\boldsymbol{k}$ and (ii) two states with the same compatibility relation into a given $\boldsymbol{k}^*$ being able to hybridize, hence forbidding symmetry-protected band crossings. Applying rules 1 and 2, we readily conclude that any isolated four-band subspace (i.e., separated by an energy gap) realizes two distinct permutations of Table I over $\mathcal{B}_\Gamma$, no more, no less. This leads to two new Dirac points (apart from the crossings at X_i) somewhere along one of the lines $\{\overline{\Gamma X_i}\}$, with i determined only by the order in energy of the IRREPs at Γ. These two Dirac points are protected by the global band topology. In Fig. 1(c) we provide a four-band tight-binding example with these two Dirac points (red) on $\overline{\Gamma Z}$.

Next, we consider the $\mathcal{B}_R$ subspace. Labeling the bands at U_i as $E^n_l(U_i)$, with $l=5,6$, and again assuming the smooth gauge, we write as $\mathcal{P}_{\overline{U_i b_j}}=(l_1l_2)$ the two-by-two permutation in energy of the two bands $\{E^{n_1}_{l_1},E^{n_2}_{l_2}\}$ under a shift from U_i by $\boldsymbol{b}_j \parallel \overline{RU_i}$. We then get *rule 3: All the bands are permuted along each line of $\mathcal{B}_R$ according to $\mathcal{P}_{\overline{Sb_3}}=\mathcal{P}_{\overline{Tb_1}}=\mathcal{P}_{\overline{Ub_2}}=(56)$.* These band permutations enforces one symmetry-protected Dirac point along each line $\overline{RU_i}$, since the two bands $\{5,6\}$ correspond to distinct IRREPs on these lines [see Fig. 1(b)]. Because of the D_2 symmetry of the midpoint R, these crossings will always be at R, leading to a fourfold degeneracy, as indicated in green in Fig. 1(c). Similarly to rule 2, we finally have *rule 4: For any two bands $E^{n_1}_{l_1}$ and $E^{n_2}_{l_2}$ at U_i with the same IRREPs, i.e., $l_1=l_2$, we have*

$$E^{n_1}_{l_1}(U_i) \gtrless E^{n_2}_{l_1}(U_i) \Leftrightarrow E^{n_1}_{l_1}(\boldsymbol{k}^*) \gtrless E^{n_2}_{l_1}(\boldsymbol{k}^*), \quad \forall \boldsymbol{k}^* \in \overline{RU_i}.$$

Together, rules 3 and 4 fully determine the global band structure in the $\mathcal{B}_R$ subspace.

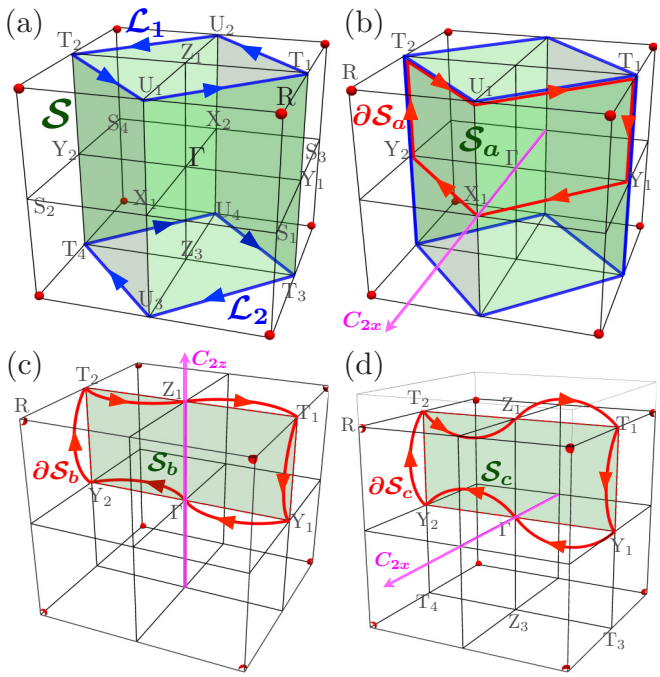

FIG. 2. (a) Closed surface $\mathcal{S}$ separating subspaces $\mathcal{B}_\Gamma$ and $\mathcal{B}_R$ with the oriented boundary $\partial\mathcal{S}=\mathcal{L}_1+\mathcal{L}_2$. (b) Oriented boundary $\partial\mathcal{S}_a$ of a subset $\mathcal{S}_a$ with $\mathcal{S}=\cup_{g\in D_2} g\mathcal{S}_a$. (c) Oriented boundary $\partial\mathcal{S}_b$ of the closed surface $\mathcal{S}'=\mathcal{S}_b+C_{2z}\mathcal{S}_b$ surrounding $h\overline{\Gamma Z}$. (d) Oriented boundary $\partial\mathcal{S}_c$ of the closed surface $\mathcal{S}''=\cup_{g\in D_2} g\mathcal{S}_c$ surrounding the plane $\overline{X}$. In (c) and (d), $\mathcal{S}_{(b,c)}$ is obtained from the green plane through a smooth inflation out of plane with the oriented boundary $\partial\mathcal{S}_{(b,c)}$ constrained by the symmetry requirement that $\mathcal{S}_{(b,c)}+C_{2(z,x)}\mathcal{S}_{(b,c)}$ is closed.

Left to consider is the $\mathcal{B}_{\Gamma\text{-}R}$ subspace, but here only one 2D IRREP is allowed, which excludes any extra symmetry-protected Dirac points. The whole $4N$-band structure can thus be determined by knowing the energy ordering of the IRREPs at the high-symmetry points $\{\Gamma,S,T,U\}$. Figure 3 gives two eight-band examples where these rules give the full band structure.

Four-band topology. Having demonstrated the existence of Dirac band-crossing points, we turn to fully characterizing their topology. We start with the simplest four-band case. For this we derive the Chern number of each Dirac point algebraically, i.e., with no other assumption than that the system satisfies SG19. In the following, we arbitrarily split the four bands into two valence bands (occupied) and two conduction bands (unoccupied) over the whole BZ [29].

Let us first separate the two subspaces $\mathcal{B}_\Gamma$ and $\mathcal{B}_R$ by the green box $\mathcal{S}$ shown in Fig. 2(a). $\mathcal{S}$ is chosen such that it is closed (the oriented boundaries $\partial\mathcal{S}=\mathcal{L}_1+\mathcal{L}_2\cong 0$ due to periodicity), symmetric under D_2, and supporting a fully gapped spectrum. Effectively, $\mathcal{S}$ surrounds $\mathcal{B}_\Gamma$. Any smooth

deformation of $\mathcal{S}$ satisfying these conditions and conserving the vertices also works. By Stokes' theorem the Chern number over the closed manifold $\mathcal{S}$ is simply given by the Berry phase over its boundary $\partial\mathcal{S}$, i.e., $2\pi C_1[\mathcal{S}] = \gamma[\partial\mathcal{S}]$. Notice that we here have to assume a smooth gauge, such that the Berry phase γ varies smoothly as we sweep the loop $\mathcal{L}$ over $\mathcal{S}$ [31]. Next, we rewrite $\mathcal{S}$ as the orbit of a subset $\mathcal{S}_a$ under the point group D_2, i.e., $\mathcal{S} = \bigcup_{g\in D_2} g\mathcal{S}_a$. Using the symmetry of the Berry curvature under D_2[30], we then have the simplification $2\pi C_1[\mathcal{S}] = 4\gamma[\partial\mathcal{S}_a]$, with $\partial\mathcal{S}_a$ the red oriented loop shown in Fig. 2(b). We are thus left with the task of evaluating the Berry phase $\gamma[\partial\mathcal{S}_a]$.

The total Abelian Berry phase of the valence (occupied) subspace of a closed loop $\mathcal{L}$ is given by $e^{-i\gamma[\mathcal{L}]} = \det \mathcal{W}[\mathcal{L}]$, where $\mathcal{W}[\mathcal{L}]$ is the matrix (non-Abelian) Wilson loop computed in the valence band basis $|\boldsymbol{u}_{\rm occ},\boldsymbol{k}\rangle = (|u_{v_1},\boldsymbol{k}\rangle,|u_{v_2},\boldsymbol{k}\rangle)^T$ [27]. We can then decompose the loop $\partial\mathcal{S}_a$ into segments with high-symmetry end points: $\mathcal{W}[\partial\mathcal{S}_a] = \mathcal{W}_{X_1\leftarrow Y_1}\mathcal{W}_{Y_1\leftarrow T_1}\mathcal{W}_{T_1\leftarrow U_1}\mathcal{W}_{U_1\leftarrow T_2}\mathcal{W}_{T_2\leftarrow Y_2}\mathcal{W}_{Y_2\leftarrow X_1}$ [see Fig. 2(b)]. A symmetry reduction based on C_{2x}, assuming that the half $\mathcal{S}_a + C_{2x}\mathcal{S}_a$ of $\mathcal{S}$ is closed, using techniques developed in Refs. [32–35], then gives [27]

$$\det \mathcal{W}[\partial\mathcal{S}_a] = \det\left[\check{S}_x^X \cdot \left(\check{S}_x^Y\right)^{-1} \cdot \check{S}_x^T \cdot \left(\check{S}_x^U\right)^{-1}\right] = \prod_{n=1,2} \frac{\lambda_{x,n}^X \lambda_{x,n}^T}{\lambda_{x,n}^Y \lambda_{x,n}^U}. \quad (1)$$

Here, $\check{S}_x^{\boldsymbol{k}^*} = \langle \boldsymbol{u}_{\rm occ},C_{2x}\boldsymbol{k}^*|\{C_{2x}|\boldsymbol{\tau}_x\}|\boldsymbol{u}_{\rm occ},\boldsymbol{k}^*\rangle$ gives a representation of the symmetry operator $\{C_{2x}|\boldsymbol{\tau}_x\}$ in the occupied band basis at the high-symmetry point $C_{2x}\boldsymbol{k}^* = \boldsymbol{k}^* - \boldsymbol{K}[C_{2x}]$ ($\boldsymbol{K}[C_{2x}]$ is a reciprocal lattice vector, possibly zero) with $\lambda_{x,n}^{\boldsymbol{k}^*}$ being its nth eigenvalue. Since the eigenvalues are invariant under (unitary) basis changes we can readily use tabulated IRREPs [18,26] and we find $e^{-i\gamma[\partial\mathcal{S}_a]} = \det \mathcal{W}[\partial\mathcal{S}_a] = -1$ and thus the Chern number $C_1[\mathcal{S}] = 4\gamma[\partial\mathcal{S}_a]/(2\pi) = 2 \mod 4$ [36]. We thus conclude that there is a symmetry-protected obstruction to the realization of a trivial insulating band structure over $\mathcal{S}$, leading to the existence of topologically stable Dirac points in $\mathcal{B}_\Gamma$. Choosing the smallest Berry phase, we get $C_1[\mathcal{B}_\Gamma] = \pm 2$. By the cancellation of the global charge (Nielsen-Ninomiya theorem [37–39]), the Chern number of $\mathcal{B}_R \subset BZ\backslash\mathcal{B}_\Gamma$ must then be $C_1[\mathcal{B}_R] = \mp 2$ and hence the R point is necessarily a double Dirac point.

We now establish that the above result can be refined by choosing tighter "boxes." First, we consider a closed surface $\mathcal{S}'$ that surrounds half of a line of $\mathcal{B}_\Gamma$ (written $h\overline{\Gamma X_i}$) and is symmetric under a C_{2i} rotation around that axis [see, e.g., Fig. 2(c) for $\mathcal{S}' = \mathcal{S}_b + C_{2z}\mathcal{S}_b$ surrounding $h\overline{\Gamma Z}$]. Following a similar line of thought as above, the Chern number is given by the Berry phase of the surface boundary. Further proceeding with a symmetry reduction of the Wilson loop based on C_{2i}, we find [27]

$$e^{-i\pi C_1[h\overline{\Gamma X_i}]} = -\chi_i^{v_1}\chi_i^{v_2}, \quad (2)$$

where $\chi_i^{v_n}$ ($=\lambda_{i,v_n}^{\boldsymbol{0}}$) is the character of the 1D IRREP $\Gamma_{v_n}^{\boldsymbol{0}}(\{C_{2i}|\boldsymbol{\tau}_i\})$ of the valence band v_n at Γ, given in Fig. 1(b). Therefore, depending on the valence IRREPs at Γ, we either have $C_1[h\overline{\Gamma X_i}] = 0 \mod 2$ such that no Dirac point is present, or $C_1[h\overline{\Gamma X_i}] = 1 \mod 2$, which gives the existence of a simple Dirac point ($|C_1| = 1$) on the half line $h\overline{\Gamma X_i}$.

TABLE II. The three inequivalent band topologies of $\mathcal{B}_\Gamma$ given by the Chern numbers of its half lines ($h\overline{\Gamma X_i}$) and planes ($\overline{X_i}$) for eight bands with four valence bands.

$\Gamma_{\rm I}$: $\{\Gamma_1,\Gamma_2,\Gamma_3,\Gamma_4\}$	$C_1[h\overline{\Gamma X_i}] = \frac{C_1[\overline{X_i}]}{2} = 0 \mod 2$
$\Gamma_{\rm II}$: $\{\Gamma_j,\Gamma_j,\Gamma_k,\Gamma_l\}_{j\neq k\neq l}$	$e^{-i\pi C_1[h\overline{\Gamma X_i}]} = e^{-i\pi\frac{C_1[\overline{X_i}]}{2}} = \chi_i^k\chi_i^l$
$\Gamma_{\rm III}$: $\{\Gamma_j,\Gamma_j,\Gamma_k,\Gamma_k\}_{j\neq k}$	$e^{-i\pi\frac{C_1[h\overline{\Gamma X_i}]}{2}} = -\chi_i^j\chi_i^k$
	$e^{-i\pi\frac{C_1[\overline{X_i}]}{4}} = +\chi_i^j\chi_i^k$

Next, we instead choose a closed surface $\mathcal{S}'' = \bigcup_{g\in D_2} g\mathcal{S}_c$ that surrounds the plane containing Γ and perpendicular to the line $\overline{\Gamma X_i}$ (written $\overline{X_i}$). The Chern number is then given by $2\pi C_1[\overline{X_i}] = 4\gamma[\partial\mathcal{S}_c]$, as illustrated for $\overline{X}$ in Fig. 2(d). Finally, the symmetry reduction of the Wilson loop based on C_{2i}, assuming that the half $\mathcal{S}_c + C_{2i}\mathcal{S}_c$ of $\mathcal{S}''$ is closed, gives [27]

$$e^{-i\frac{\pi C_1[\overline{X_i}]}{2}} = +\chi_i^{v_1}\chi_i^{v_2}. \quad (3)$$

Thus, depending on the valence IRREPs at Γ, we either have $C_1[\overline{X_i}] = 0 \mod 4$, i.e., no Dirac points on $\overline{X_i}$, or $C_1[\overline{X_i}] = 2 \mod 4$, demonstrating that the two simple Dirac points on the plane $\overline{X_i}$ have the same charge. This result also directly implies that the R Dirac point has charge ∓ 2. This fully characterizes the global band topology of any four-band subspace with SG19 [40].

Eight-band topology. We next consider the topology of eight bands. Similarly to before, we arbitrarily split the bands into four valence and four conduction bands over the whole BZ. We then find the Chern numbers corresponding to Eqs. (2) and (3) as

$$e^{-i\pi C_1[h\overline{\Gamma X_i}]} = (-1)^2\chi_i^{v_1}\chi_i^{v_2}\chi_i^{v_3}\chi_i^{v_4}, \quad (4)$$

$$e^{-i\pi\frac{C_1[\overline{X_i}]}{2}} = (+1)^2\chi_i^{v_1}\chi_i^{v_2}\chi_i^{v_3}\chi_i^{v_4}. \quad (5)$$

Both are thus still determined by the valence IRREPs at Γ. From Eqs. (4) and (5) we identify three topologically inequivalent classes of band structures over $\mathcal{B}_\Gamma$. This leads to Table II [41]. $\Gamma_{\rm I}$ excludes simple Dirac points within $\mathcal{B}_\Gamma$. $\Gamma_{\rm II}$ enforces two pairs of same-charge simple Dirac points within $\mathcal{B}_\Gamma$ with a total charge of 0 or |4|. $\Gamma_{\rm III}$ has one quadruple of (same-charge) simple Dirac points on a single line in $\mathcal{B}_\Gamma$.

We also have to characterize the topology of $\mathcal{B}_R$. We find for the three half lines in $\mathcal{B}_R$ (written $\{h\overline{RU_i}\}$) [27]

$$e^{-i\pi C_1[h\overline{RU_i}]} = (-1)^2 \det\left[\Gamma_{v_1}^{U_i}(C_{2i})\Gamma_{v_2}^{U_i}(C_{2i})\right]. \quad (6)$$

Thus two inequivalent situations can be realized according to if $\Gamma_{v_1}^{U_i} = \Gamma_{v_2}^{U_i}$ or $\Gamma_{v_1}^{U_i} \neq \Gamma_{v_2}^{U_i}$. From this we derive Table III [42]. In both cases the Chern numbers of the planes containing R and perpendicular to the axes $\{\overline{RU_i}\}$ (written $\overline{U_i}$) are [27]

TABLE III. The two inequivalent band topologies of $\mathcal{B}_R$ given by the Chern numbers of its half-lines ($h\overline{RU_i}$) and planes ($\overline{U_i}$) for eight bands with four valence bands.

$U_{i,\rm I}$: $\{\Gamma_5,\Gamma_6\}$	$C_1[h\overline{RU_i}] = \frac{C_1[\overline{U_i}]}{2} = 0 \mod 2$
$U_{i,\rm II}$: $\{\Gamma_j,\Gamma_j\}$	$C_1[h\overline{RU_i}] = \frac{C_1[\overline{U_i}]}{2} = 2 \mod 4$

TABLE IV. The eight nonequivalent band topological classes for eight bands with four valence bands. $[(\cdot)]$ means the equivalence class obtained by cyclic permutations of S,T,U.

Γ_{I}	Γ_{II}	Γ_{III}
$(S_{\mathrm{I}},T_{\mathrm{I}},U_{\mathrm{I}})$	$(S_{\mathrm{I}},T_{\mathrm{I}},U_{\mathrm{I}})$	$[(S_{\mathrm{II}},T_{\mathrm{I}},U_{\mathrm{I}})]$
$[(S_{\mathrm{II}},T_{\mathrm{II}},U_{\mathrm{I}})]$	$[(S_{\mathrm{II}},T_{\mathrm{I}},U_{\mathrm{I}})]$	$(S_{\mathrm{II}},T_{\mathrm{II}},U_{\mathrm{II}})$
	$[(S_{\mathrm{II}},T_{\mathrm{II}},U_{\mathrm{I}})]$	
	$(S_{\mathrm{II}},T_{\mathrm{II}},U_{\mathrm{II}})$	

$C_1[\overline{U_i}] = 0 \mod 4$. Thus, the class $U_{i,\mathrm{I}}$ corresponds to a band structure with no double Dirac point on the half line $h\overline{RU_i}$, while the class $U_{i,\mathrm{II}}$ has a pair of (same-charge) double Dirac points on the line $\overline{RU_i}$.

The band structure of any eight bands is fully characterized in terms of the classes $\{\Gamma_{\mathrm{I}},\Gamma_{\mathrm{II}},\Gamma_{\mathrm{III}}\}$ for $\mathcal{B}_\Gamma$ and $\{S_{\mathrm{I}},S_{\mathrm{II}},T_{\mathrm{I}},T_{\mathrm{II}},U_{\mathrm{I}},U_{\mathrm{II}}\}$ for $\mathcal{B}_R$. The classes are in turn determined by the energy-ordered IRREPs at the high-symmetry points $\{\Gamma,S,T,U\}$. While we argued that the two subspaces $\mathcal{B}_\Gamma$ and $\mathcal{B}_R$ are symmetry independent, they are actually constrained by a global charge cancellation over the whole BZ. Enumerating all the combinatorial possibilities up to the charge cancellation requirement results in the eight inequivalent band topological classes presented in Table IV.

A band-structure example from class $(\Gamma_{II},S_I,T_I,U_I)$ is shown in Fig. 3(a). It realizes two pairs of simple Dirac points (blue): one pair on $\overline{\Gamma Y}$ (both with charge ±1) and one on $\overline{\Gamma Z}$ (both with charge ∓1). These new Dirac points are in addition to those found above within the four band subspaces (red and green). Density functional theory (DFT) band structures of three-dimensional (3D) organic materials with SG19 belonging to the same class have also recently been found [43]. Another example from class $(\Gamma_{\mathrm{III}},S_{\mathrm{II}},T_{\mathrm{I}},U_{\mathrm{I}})$ is shown in Fig. 3(b). It realizes a quadruple of simple Dirac points (blue) on $\overline{\Gamma Z}$ (all of charge ∓1) and a pair of double Dirac points (purple) on $\overline{RS}$ (both of charge ±2).

The technique illustrated above can be straightforwardly extended to arbitrary $4N$-band structures. Simply, from the list of energy-ordered IRREPs at $\{\Gamma,S,T,U\}$ we can thus deduce the global band topology and predict all simple and double Dirac points protected by symmetry. In addition, at integer filling the number of valence bands must be a multiple of 2 and the IRREP ordering determines if the material is an insulator (the filling number is then a multiple of 4) or a topological semimetal, where the Fermi level necessarily crosses the bands forming Dirac points. In fact, due to global charge cancellation, distinct sets of Dirac points, not connected by point symmetry, are necessarily realized, such that the Fermi level generally does not cross at the point nodes [see, e.g., Fig. 1(c)]. This leads to "Dirac-point metals" (the point-nodal analog to Ref. [14]). A true semimetallic state is only achieved through fine tuning of the band structure. The generality of the technique also means that it is not restricted to SG19 and it can also easily be generalized to include spin degrees of freedom. The strong explicative and predictive power in combining symmetry and topology makes this algebraic approach highly complementary to current data mining searches for topological semimetals [44,45] and can place it at the core of future intelligent DFT-based data mining schemes.

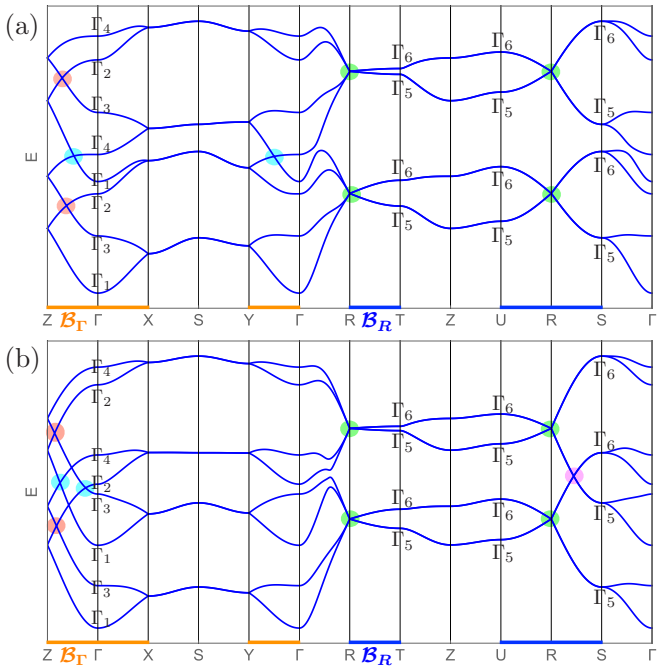

FIG. 3. Electronic band structure of eight-band tight-binding models in SG19, corresponding to (a) class $(\Gamma_{\mathrm{II}},S_{\mathrm{I}},T_{\mathrm{I}},U_{\mathrm{I}})$ and (b) class $(\Gamma_{\mathrm{III}},S_{\mathrm{II}},T_{\mathrm{I}},U_{\mathrm{I}})$. Symmetry-protected single Dirac points ($|C_1|=1$) globally unavoidable in red (as obtained in the four-band subspace) and class dependent in blue for an eight-band subspace, as well as double Dirac points ($|C_1|=2$) globally unavoidable in green (as in the four-band subspace) and class dependent in purple (eight-band subspace).

Note added. Recently, we became aware of Refs. [46,47], which consider global topological classification. While some conclusions are similar to ours (especially the former that also considers a 3D example), their derivations are more formal (making use of K theory) and they both exclude time-reversal symmetry. Our approach is more heuristic and importantly includes time-reversal symmetry, which is usually present in the normal state.

Acknowledgments. We thank M. Geilhufe, A. Balatsky, and S. Borysov for useful discussions. The first author thanks A. Furusaki for an insightful discussion in the early stage of the work. This work was supported by the Swedish Research Council (Vetenskapsrådet) and the Knut and Alice Wallenberg Foundation.

[1] C.-K. Chiu, J. C. Teo, A. P. Schnyder, and S. Ryu, Rev. Mod. Phys. **88**, 035005 (2016).

[2] S. M. Young, S. Zaheer, J. C. Y. Teo, C. L. Kane, E. J. Mele, and A. M. Rappe, Phys. Rev. Lett. **108**, 140405 (2012).

[3] B.-J. Yang and N. Nagaosa, Nat. Commun. **5**, 4898 (2014).

[4] C.-K. Chiu and A. P. Schnyder, Phys. Rev. B **90**, 205136 (2014).

[5] B.-J. Yang, T. Morimoto, and A. Furusaki, Phys. Rev. B **92**, 165120 (2015).

[6] B. J. Wieder, Y. Kim, A. M. Rappe, and C. L. Kane, Phys. Rev. Lett. **116**, 186402 (2016).
[7] K. Shiozaki and M. Sato, Phys. Rev. B **90**, 165114 (2014).
[8] S. M. Young and C. L. Kane, Phys. Rev. Lett. **115**, 126803 (2015).
[9] Y. Kim, B. J. Wieder, C. L. Kane, and A. M. Rappe, Phys. Rev. Lett. **115**, 036806 (2015).
[10] K. Shiozaki, M. Sato, and K. Gomi, Phys. Rev. B **91**, 155120 (2015).
[11] K. Shiozaki, M. Sato, and K. Gomi, Phys. Rev. B **93**, 195413 (2016).
[12] B.-J. Yang, T. A. Bojesen, T. Morimoto, and A. Furusaki, Phys. Rev. B **95**, 075135 (2017).
[13] B. J. Wieder and C. L. Kane, Phys. Rev. B **94**, 155108 (2016).
[14] T. Bzdusek, Q. S. Wu, A. Rüegg, M. Sigrist, and A. A. Soluyanov, Nature (London) **538**, 75 (2016).
[15] Y. X. Zhao and A. P. Schnyder, Phys. Rev. B **94**, 195109 (2016).
[16] G. Chang, D. S. Sanchez, B. J. Wieder, S.-Y. Xu, F. Schindler, I. Belopolski, S.-M. Huang, B. Singh, D. Wu, T. Neupert, T.-R. Chang, H. Lin, and M. Z. Hasan, arXiv:1611.07925.
[17] R. M. Geilhufe, A. Bouhon, S. S. Borysov, and A. V. Balatsky, Phys. Rev. B **95**, 041103 (2017).
[18] C. Bradley and A. Cracknell, *The Mathematical Theory of Symmetry in Solids* (Oxford University Press, Oxford, UK, 1972).
[19] L. Michel and J. Zak, Phys. Rev. B **59**, 5998 (1999).
[20] L. Michel and J. Zak, Europhys. Lett. **50**, 519 (2000).
[21] J. Zak, J. Phys. A: Math. Gen. **35**, 6509 (2002).
[22] G. Lee, J. S. Kim, and J. Zak, J. Phys.: Condens. Matter **15**, 2005 (2003).
[23] H. Watanabe, H. C. Po, M. P. Zaletel, and A. Vishwanath, Phys. Rev. Lett. **117**, 096404 (2016).
[24] In this work we neglect spin-orbit coupling and use a fully spin-polarized description, but otherwise assume time-reversal symmetry (TRS). A brief discussion of breaking TRS is included in the Supplemental Material [27].
[25] Each lattice site has three inequivalent partners under screw symmetries with which they form a basis for each of the four IRREPs of D_2 (see SM [27]).
[26] M. I. Aroyo, A. Kirov, C. Capillas, J. M. Perez-Mato, and H. Wondratschek, Acta Crystallogr., Sect. A **62**, 115 (2006).
[27] See Supplemental Material at http://link.aps.org/supplemental/10.1103/PhysRevB.95.241101 for a brief introduction in representation theory and symmetry based tight-binding modeling. It also gives a proof of the band permutation rules. The details of the algebraic derivation of the Chern numbers are given and the numerical computation of simple and double Dirac point Chern numbers are also shown, which includes Refs. [48–52].
[28] Note that these crossings are actually part of twofold degenerate lines over the whole $\mathcal{B}_{\Gamma\text{-}R}$ subspace.
[29] Strictly speaking, this band-splitting procedure would require a $\boldsymbol{k}$-dependent Fermi level, but as a conceptual tool it is still valid.
[30] Writing the Berry curvature as $\boldsymbol{\mathcal{F}}$ and the (matrix) Berry-Wilczek-Zee connection as $\boldsymbol{\mathcal{A}}$, we have $2\pi C_1[\mathcal{S}] = \int_{\mathcal{S}} \boldsymbol{\mathcal{F}} \cdot d\boldsymbol{s} = \sum_{g\in D_2} \int_{g\mathcal{S}_a} \boldsymbol{\mathcal{F}} \cdot d\boldsymbol{s} = 4 \int_{\mathcal{S}_a} \boldsymbol{\mathcal{F}} \cdot d\boldsymbol{s} = 4 \oint_{\partial\mathcal{S}_a} \mathrm{Tr}\boldsymbol{\mathcal{A}} \cdot d\boldsymbol{l} = 4\gamma[\partial\mathcal{S}_a]$.
[31] The smooth gauge guarantees that if $\mathcal{S}$ is a nontrivial manifold, i.e., surrounding a topologically stable band crossing, then $\gamma[\mathcal{L}_1]$ and $\gamma[\mathcal{L}_2^{-1}]$ belong to different sectors (separated by $2n\pi$) and thus the phase difference $\gamma[\mathcal{L}_1] + \gamma[\mathcal{L}_2] = \gamma[\mathcal{L}_1] - \gamma[\mathcal{L}_2^{-1}]$ is not trivially zero, even though $\mathcal{L}_1 + \mathcal{L}_2 \cong 0$, leading to a Chern number $C_1 = n$. See also Refs. [36,40].
[32] T. L. Hughes, E. Prodan, and B. A. Bernevig, Phys. Rev. B **83**, 245132 (2011).
[33] C. Fang, M. J. Gilbert, and B. A. Bernevig, Phys. Rev. B **86**, 115112 (2012).
[34] Z. Wang, A. Alexandradinata, R. Cava, and B. A. Bernevig, Nature (London) **532**, 189 (2016).
[35] A. Alexandradinata and B. A. Bernevig, Phys. Rev. B **93**, 205104 (2016).
[36] The Chern number is here obtained through an absolute Berry phase, hence inheriting the torsor structure of a phase, i.e., without a favored trivial element as the mod 4 ambiguity shows. See SM [27] for (numerical) calculations of the Chern number through the total flow of the Berry phase, i.e., now a phase difference, eliminating this ambiguity.
[37] H. Nielsen and M. Ninomiya, Nucl. Phys. B **185**, 20 (1981).
[38] H. Nielsen and M. Ninomiya, Nucl. Phys. B **193**, 173 (1981).
[39] E. Witten, Riv. Nuovo Cimento **39**, 313 (2016).
[40] The SM [27] contains a numerical computation of the Chern number of simple and double Dirac points for an explicit four-band tight-binding model that confirms the general results.
[41] Γ_{III} is found by taking the square root of Eqs. (4) and (5).
[42] $U_{i,\mathrm{II}}$ is found by taking the square root of Eq. (6).
[43] R. M. Geilhufe, S. S. Borysov, A. Bouhon, and A. V. Balatsky, arXiv:1611.04316 .
[44] S. S. Borysov, R. M. Geilhufe, and A. V. Balatsky, PLoS ONE **12**, e0171501 (2017).
[45] R. Chen, H. C. Po, J. B. Neaton, and A. Vishwanath, arXiv:1611.06860 .
[46] J. Kruthoff, J. de Boer, J. van Wezel, C. L. Kane, and R.-J. Slager, arXiv:1612.02007 .
[47] K. Shiozaki, M. Sato, and K. Gomi, arXiv:1701.08725 .
[48] D. Brink and G. Satchler, *Angular Momentum* (Oxford University Press, Oxford, UK, 1993).
[49] M. Lax, *Symmetry Principles in Solid States and Molecular Physics* (Dover, New York, 1973).
[50] A. Stone, Proc. R. Soc. London, Ser. A **351**, 141 (1976).
[51] R. Yu, X. L. Qi, A. B. Bernevig, Z. Fang, and X. Dai, Phys. Rev. B **84**, 075119 (2011).
[52] H. Weng, R. Yu, X. Hu, X-Dai, and Z. Fang, Adv. Phys. **64**, 227 (2015).